

Triphenylene Columnar Liquid Crystals: Excited States and Energy Transfer

Dimitra Markovitsi,^{*,†} Arnaud Germain,[‡] Philippe Millié,[‡] and Pierre Lécuyer[†]

Centre d'Etudes de Saclay, CEA, DRECAM, 91191 Gif-sur-Yvette, France

Lazaros K. Gallos and Panos Argyrakis

Department of Physics, University of Thessaloniki, 54006 Thessaloniki, Greece

Holger Bengs[§] and Helmut Ringsdorf

Institut für Organische Chemie, Universität Mainz J. J. Becher-Weg 18-20, 55099 Mainz, Germany

Received: June 22, 1994; In Final Form: October 21, 1994[®]

The present paper deals with the photophysical properties of columnar liquid crystals formed by hexakis(alkyloxy)triphenylenes. Absorption and fluorescence spectra of solutions are analyzed on the basis of quantum chemical calculations performed by the CS-INDO-CI (conformations spectra–intermediate neglect of differential overlap–configuration interaction) method: the absorption maximum is due to the $S_0 \rightarrow S_4$ transition while fluorescence originates from the weak $S_0 \rightarrow S_1$ transition. In columnar aggregates, the former transition corresponds to delocalized excited states while the latter corresponds to localized ones; calculation of intermolecular interactions shows that, at the temperature domain of the mesophases, all the molecules have the same excitation energy and, therefore, no spectral diffusion of the fluorescence is expected, in agreement with the time-resolved emission spectra. Excitation transfer is investigated by studying the fluorescence decays of mesophases doped with energy traps. Their analysis is made by means of Monte Carlo simulations considering both intracolumnar and intercolumnar jumps and using four different models for the distance dependence of the hopping probability. The best description is obtained with a model based on the extended dipole approximation and taking into account molecular orientation.

1. Introduction

Columnar liquid crystals are molecular materials characterized by a highly anisotropic structure. They are usually composed of disklike molecules containing a rigid core surrounded by equatorial flexible chains.^{1–5} Their structure corresponds to stacks of molecular disks forming columns. The intercolumnar distance is 20–40 Å, depending on the lateral chain length, while the stacking distance is less than 4.5 Å. Therefore, interactions between neighboring molecules within the same column should be much stronger than interactions between neighboring columns. Consequently, transport phenomena (excitation or charge) are expected to be quasi one-dimensional. In this context, several papers published in the past few years report the photophysical and electrical properties of columnar mesophases.^{6–16}

In particular, it has been suggested that excitation energy transport in columnar liquid crystals can be used as a mode of signal transmission in molecular electronics.^{11,12} For practical applications of such “molecular energy guides”, the temporal and spatial evolution of the excitation has to be elucidated. This aspect greatly depends on whether the excited states involved in the transport process are localized or delocalized. Two publications dealing with the dynamic behavior of excited triplet and singlet states assume hopping of localized excitations. They report that a one-dimensional random walk model gives a good description of the decays of the excited states recorded for phthalocyanine and triphenylene mesophases.^{11,12} The fitting

of the experimental decays with theoretical ones provides an order of magnitude for the hopping time to the nearest neighbor: 0.4–60 ps for the phthalocyanine triplet¹¹ and *ca.* 30 fs for the triphenylene singlet.¹² The latter value is very intriguing because it corresponds to strong interactions and thus possibly to delocalized excited states. As a matter of fact, a recent study of the spectroscopic properties of the columnar liquid crystals formed by triaryl pyrylium salts has shown that delocalized excited states may exist in these systems even at room temperature.^{17,18}

In order to obtain a better insight into the nature of the excited states and the energy transfer processes, we have undertaken an experimental and theoretical investigation of 2,3,6,7,10,11-hexakis(*n*-alkyloxy)triphenylenes (Figure 1) having different lateral alkyloxy chains: pentyloxy (H5T), heptyloxy (H7T), and nonyloxy (H9T). In their liquid crystalline phases, the stacking distance *d* is 3.6 Å while the intercolumnar distance *D* is 20.2, 22.6, and 24.3 Å for H5T, H7T, and H9T, respectively.¹⁶ For the purpose of comparison, we also studied the properties of the hexakis(methyloxy) (H1T) derivative, which does not form any mesophase. The experimental work had one important limitation inherent in the examined systems: they are stable only at given temperature domains (69–122 °C for H5T, 69–93 °C for H7T, 57–78 °C for H9T). Upon cooling, crystallization occurs and all the properties of the columnar mesophases disappear. Therefore, it is impossible to perform low-temperature experiments yielding precious information about the questions we addressed. In order to palliate this difficulty, our experimental results obtained at high temperature were analyzed in the light of theoretical models.

For the characterization of the excited states of the isolated chromophore we carried out quantum chemistry calculations according to the CS-INDO-CI (conformations spectra–inter-

[†] SCM, CNRS-URA 331, Laboratoire de Photophysique et Photochimie.

[‡] SPAM, Laboratoire de Chimie Théorique.

[§] Present address: Hoechst AG, Central Research G 830, 65926 Frankfurt a. M., Germany.

[®] Abstract published in *Advance ACS Abstracts*, December 15, 1994.

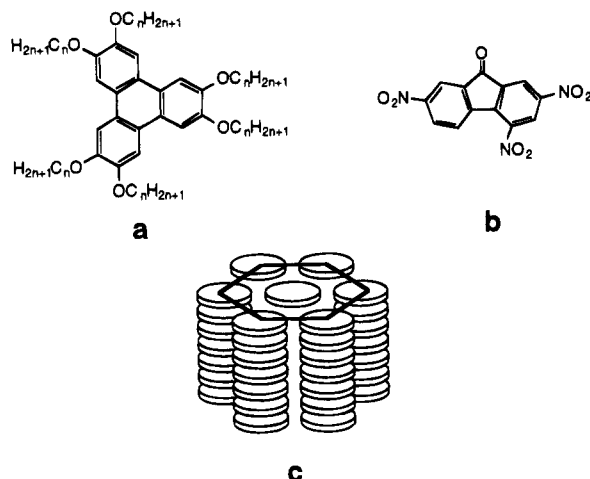


Figure 1. Schematic representation of the studied (a) 2,3,6,7,10,11-hexakis(*n*-alkyloxy)triphenylenes H1T ($n = 1$), H5T ($n = 5$), H7T ($n = 7$), and H9T ($n = 9$), (b) 2,4,7-trinitrofluoren-9-one (TNF), and (c) columnar mesophases; the stacking distance is 3.6 Å, and the intercolumnar distance is 20.2, 22.6, and 24.3 Å for H5T, H7T, and H9T, respectively.

mediate neglect of differential overlap—configuration interaction) method. Within the same formalism, we especially focused on the determination of the interactions between transition moments playing a crucial role in the energy transfer processes. The excited states of the columnar stacks were calculated in the frame of the excitonic theory combined with quantum chemistry methods. Such a methodology, initially developed for columnar aggregates of ionic compounds,¹⁷ gives the possibility to take into account complex molecular arrangements and to evaluate the influence of structural defects on the spectroscopic properties of organized molecular systems. The latter point is very important because the excitation energy of structural defects may be lower than that of the other molecules in the lattice. In that case, defect sites behave as energy traps.

For the study of the dynamical behavior of the excitation, the fluorescence decays of H n T in their columnar liquid crystalline phases doped with an energy trap were recorded. Samples with various trap concentrations were examined. The trap used was 2,4,7-trinitrofluoren-9-one (TNF, Figure 1), which forms charge transfer complexes with H n T and thus is inserted in the columnar stacks.^{19–23} The experimental decays were fitted with curves obtained by Monte Carlo simulations,^{24,25} the fitting parameter being the hopping time to the nearest neighbor. Although a great number of analytical expressions describe quite well transport phenomena in restricted geometries,²⁶ it may be inappropriate to use them for the columnar mesophases having a very specific geometry. On the contrary, Monte Carlo simulations give the possibility to take into account various factors affecting the transport properties in a precise molecular assembly.

The determination of the hopping time through a fitting procedure is an indirect method, and the result depends on the assumptions made in the modeling; very often quite different models give acceptable fittings. With this in mind, in our simulations, we eliminated a certain number of assumptions previously made in these types of studies. Instead of a one-dimensional transport chain,^{11,12} we considered a three-dimensional lattice in which hops not only to the nearest neighbors but also at long distances take place. Regarding the distance dependence of the hopping probability, we tested different models, starting from an oversimplified currently used pattern in which molecules are assimilated to points and moving

to a more sophisticated one where molecular orientation and molecular dimensions are taken into account.

In the present communication, the experimental results are presented in section 2. Section 3 deals with the analysis of the excited states. The results of the Monte Carlo simulations are shown in section 4, and the final conclusions are given in section 5.

2. Experimental Section

2.1. Synthesis of the Compounds. The 2,3,6,7,10,11-hexakis(*n*-alkyloxy)triphenylenes were synthesized according to the well-known trimerization process of the corresponding bis-(alkyloxy)benzenes.^{27,28} The commonly used solvent, 70% sulfuric acid, was replaced by dichloromethane, thus simplifying the handling of the reaction mixture.²⁸ As an example we describe below the synthesis of the nonyloxy derivative.

1,2-Dinonylbenzene (5 g, 13.8 mmol) was dissolved in 500 mL of CH₂Cl₂, and 4.5 g (27.6 mmol) FeCl₃ was added in small portions during a period of 2 h. The end of the reaction was monitored by thin layer chromatography (solvent CH₂Cl₂/light petroleum, volume ratio 3/2). After filtration of the suspension, the solution was concentrated by evaporation of about 400 mL of CH₂Cl₂. The remaining solution was diluted with the same volume (about 100 mL) of light petroleum. Silica gel (80 g) was added, and the suspension was stirred for 10 min. Subsequent filtration and removal of the solvents resulted in raw material which was purified by recrystallization, two flash chromatographies, and again a final recrystallization. All purification procedures were carried out with a CH₂Cl₂/light petroleum mixture (volume ratio 3/2). In this way, 3.0 g (2.8 mmol) of white product was obtained (60% yield).

The purity of all the compounds was checked by thin layer chromatography. Elemental analysis and ¹H-NMR data were in accordance with the given structures.

2,4,7-Trinitrofluoren-9-one (TNF) was obtained from TCI and purified by twofold recrystallization from ethyl acetate.

The H n T/TNF mixtures were prepared as follows. For each mixture, an amount of *ca.* 50 mg of the corresponding H n T was weighed accurately into a glass vessel and dissolved in approximately 1 mL of freshly distilled tetrahydrofuran. The necessary TNF quantity was added to each mixture as a standard solution. The solution was prepared by dissolving *ca.* 100 mg of TNF in 10 mL of freshly distilled tetrahydrofuran. The solution was diluted by a factor of 100. Then, 80–800 μL of this TNF solution was added to the corresponding H n T solution by means of a syringe. The solvent was evaporated at ambient conditions while stirring the mixtures. Afterward the samples were dried at 50 °C under reduced pressure.

2.2. Apparatus and Experimental Procedure. For the spectroscopic measurements of the organized phases, a few milligrams of powder compound was deposited on a quartz flow cell heated by means of a water circulator (Haake N2-B); when the liquid crystalline phase was formed, a quartz slide was pressed on the sample. The temperature at the surface of the cell was measured with a contact thermocouple.

Steady-state absorption spectra were recorded with a Cary 3E spectrophotometer. Steady-state fluorescence emission and excitation spectra were recorded with a SPEX Fluorolog-2 spectrofluorimeter. Excitation and emission spectra were corrected. For the organized phases, the exciting beam was perpendicular to the surface of the cell and fluorescence was collected at an angle of 20° with respect to the incident beam. Fluorescence quantum yields were determined using quinine sulfate in HClO₄²⁹ and not triphenylene or dimethyl-POPOP as

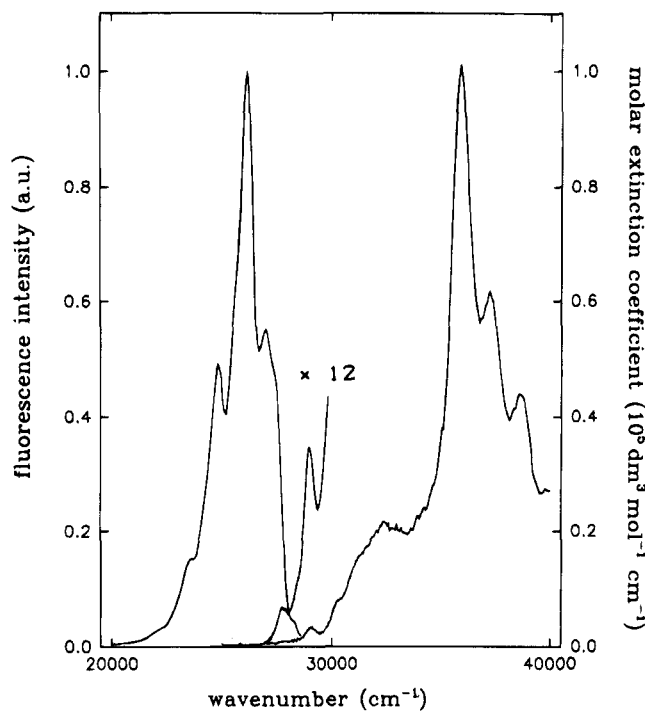


Figure 2. Room temperature absorption and fluorescence spectra of HIT in dichloromethane; $\lambda_{ex} = 344$ nm.

in ref 12 because we have found that the quantum yields of those compounds reported in the literature³⁰ are overestimated.

Time-resolved fluorescence spectra were recorded by the single-photon counting technique. The excitation source was the second harmonic of a dye laser (rhodamine 6G) synchronously pumped by a mode-locked Nd:YAG laser. A Glan-Thomson prism, forming an angle of 54.7° with the polarization direction of the exciting light (vertical), was positioned in front of the monochromator. The detector was either a photomultiplier tube (R928) or a microchannel plate (R1564U Hamamatsu), providing an instrumental response function of 800 and 150 ps (fwhm), respectively. For the measurements involving liquid crystals, fluorescence was collected at a right angle with respect to the exciting beam. Reproducible fluorescence decays were obtained only at low energy intensities. Otherwise, local heating of the sample resulted in decays becoming more and more rapid with the irradiation time; if the laser irradiation was stopped for a few minutes, the initial long decay was found again.

2.3. Properties of Hexakis(alkyloxy)triphenylenes. Absorption and fluorescence spectra of dilute HIT dichloromethane solutions are very structured (Figure 2). Such a rich structure may correspond to various electronic transitions and/or to vibrational progressions. Both spectra show only very small changes with the solvent polarity (spectral shifts < 100 cm^{-1} when going from *n*-heptane to acetonitrile). The fluorescence spectra do not depend on the excitation wavelength, and the fluorescence decays are well fitted, with a single exponential yielding a lifetime τ_f of 8.5 ns. This means that fluorescence originates only from the lowest singlet state. The excitation spectrum contains the same peaks as the absorption one but with different relative intensities (Table 1), revealing the presence of various electronic transitions. The quantum yield of internal conversion between the corresponding excited states is less than one, possibly because of intersystem crossing to triplet states.⁶ The relative intensity of the two lowest energy peaks (27 800 and 29 070 cm^{-1}) is the same in the absorption and excitation spectra. Moreover, the energy difference between them is 1270 cm^{-1} , corresponding to the aromatic C–H bending vibration.³¹ Therefore, it is reasonable to consider that they

TABLE 1: Relative Intensities of Some Peaks Appearing in the Absorption and Excitation Spectra of HIT in Dichloromethane

	peak energy, cm^{-1}				
	27 700	29 000	30 300	32 400	36 000
intensity in excitation spectrum/intensity in absorption spectrum	1.0	1.0	0.8	0.6	0.5

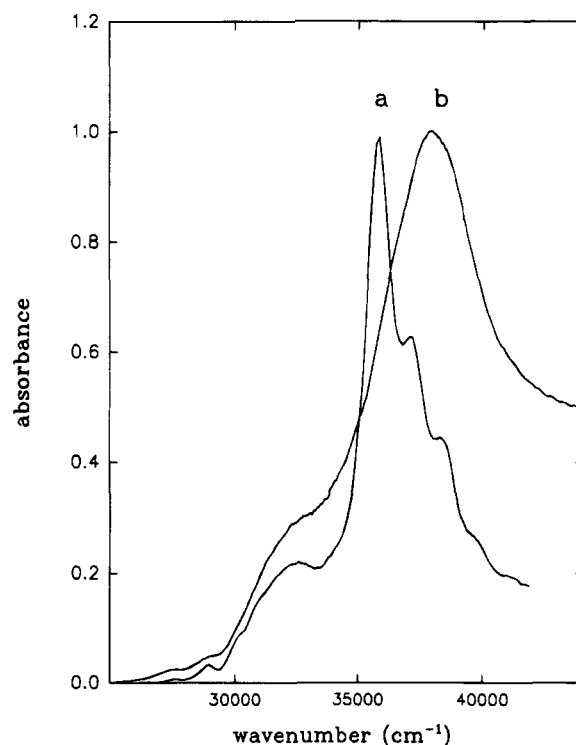


Figure 3. Absorption spectra of H5T: (a) dichloromethane solution; (b) columnar liquid crystal at 75°C .

belong to the same electronic transition $S_0 \rightarrow S_1$. The peak appearing at 28 000 cm^{-1} in the fluorescence spectrum is attributed to a hot band. The fluorescence quantum yield ϕ_f determined by excitation at 29 000 cm^{-1} is 0.068. The radiative lifetime τ_{rad} of the lowest transition, determined as τ_f/ϕ_f is 125 ns. This relatively high value of τ_{rad} shows that the transition $S_0 \rightarrow S_1$ is a rather forbidden transition which is in agreement with the weak transition moment (0.9 D) evaluated from the area for the examined peaks.

The absorption and fluorescence spectra of H_nT ($n = 5, 7, 9$) solutions are very similar to those of HIT. All three compounds have the same fluorescence lifetime ($\tau_f = 7.9$ ns in dichloromethane). Thus, the presence of long alkyl chains does not significantly affect the spectroscopic properties of the chromophore in solution. Conversely, molecular organization has an influence on the absorption spectra (Figure 3). The absorption maximum of the mesophase spectrum is blue-shifted by 2000 ± 500 cm^{-1} with respect to that of the solution spectrum; the error in the determination of the energy shift is due to the insufficient optical quality of the samples leading to light scattering. Within the spectral resolution of our experiments, the lower energy peaks of the spectra shown in Figure 3 appear at the same positions.

Figure 4 shows the normalized fluorescence spectra of H5T in benzene, in its crystalline and columnar liquid crystalline phases. Although the spectra are shifted with respect to each other, the spectrum profile determined by the vibrational structure is practically the same. The fluorescence spectra depend neither on the excitation wavelength nor on the lateral

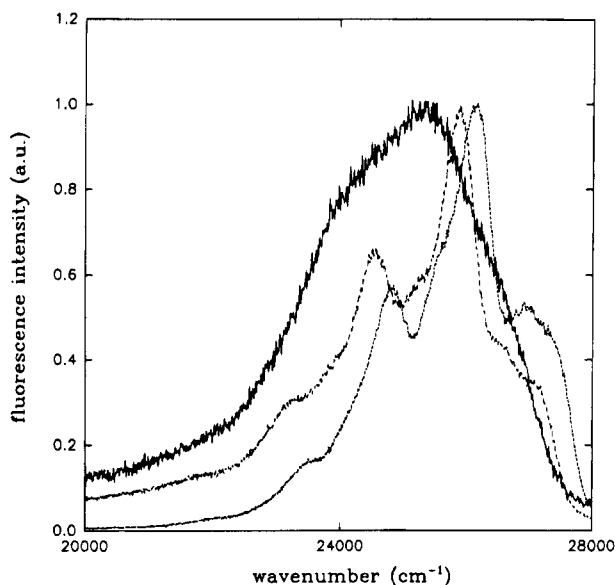


Figure 4. Normalized fluorescence spectra of H5T: (---) benzene solution; (—) crystalline phase at 20 °C; (- · -) columnar liquid crystal at 75 °C. $\lambda_{\text{ex}} = 344$ nm.

chain length, and they peak at 26 180, 25 900, and 25 200 cm^{-1} , respectively, for the solution, the solid phase, and the mesophase. It is worth noticing that the fluorescence maximum is temperature independent for the crystalline phases while for the mesophases it shifts to higher energies upon heating (an approximately 300 cm^{-1} shift for a temperature change of 30 °C).

The time-resolved fluorescence spectra of H n T ($n = 5, 7, 9$) mesophases do not depend on the time windows used. This is in agreement with the behavior of H6T previously reported.¹²

The fluorescence decays of the H5T and H7T mesophases cannot be fitted by a single exponential while that of H9T corresponds to a lifetime of 10 ns. This means that at least the first two mesophases contain intrinsic traps which could be impurities, structural defects, or oxygen. We have also recorded the decay of the fluorescence anisotropy for the H n T mesophases. A rapid depolarization occurring within the time resolution of our detection system (150 ps) is observed down to 0.1. Then the anisotropy remains constant until the end of the fluorescence decay. Energy transfer among chromophores having transition moments orthogonal to an axis leads to an anisotropy equal to 0.1. This finding suggests that, for the examined mesophases which are not oriented, energy transfer occurs only within single monodomains.

2.4. Properties of the H n T/TNF Mixtures. The absorption spectra of the H n T/TNF charge transfer complexes are shown in ref 23. Excitation at the CT band did not reveal any fluorescence. TNF shows no fluorescence either. Therefore, the only fluorescence that can be detected for H n T/TNF mixtures is that coming from H n T. However, the H n T fluorescence is completely quenched in the CT complexes. Thus, *n*-heptane solutions containing equimolar mixtures of H n T and TNF do not fluoresce at all. The same thing happens with the mesophases formed by H n T/TNF at molar ratios 1/1 or 3/1. This means that TNF is a very efficient trap for the excitation energy of H n T. The trapping process proceeds through a rapid electron transfer (<30 ps) in the CT complex.³²

We have recorded the fluorescence spectra and fluorescence decays of the H n T mesophases containing a small amount of TNF (from 10^{-5} to 5×10^{-3} molar fraction). The fluorescence spectra of these mixtures are identical to the spectra of undoped H n T mesophases. Upon increasing TNF concentration, the

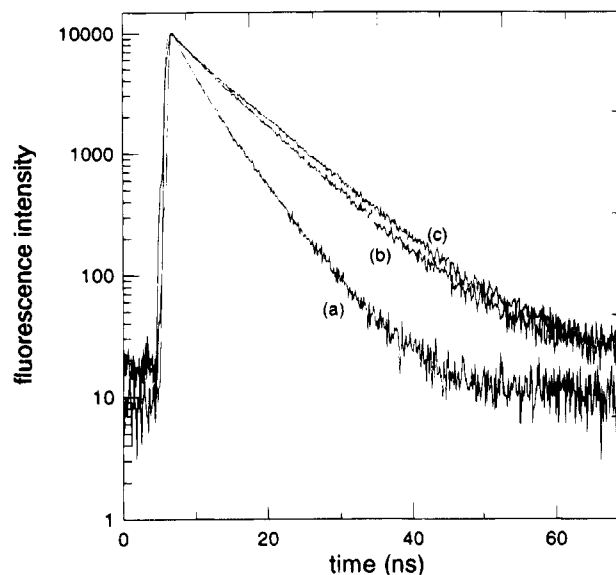


Figure 5. Fluorescence decays of H n T mesophases at 80 °C: (a) H5T; (b) H7T; (c) H9T. TNF molar fraction = 5×10^{-3} ; $\lambda_{\text{ex}} = 295$ nm; $\lambda_{\text{em}} = 400$ nm.

fluorescence intensity decreases and the fluorescence decay becomes more rapid. Such a variation becomes noticeable for TNF molar fractions of 10^{-3} , indicating that the intrinsic trap concentration is of that order of magnitude.

Figure 5 shows the dependence of the fluorescence decay on the intercolumnar distance. For the same trap concentration, the longer the lateral chains, the slower the decay. This may be due to intercolumnar energy transfer and/or to a dependence of the intracolumnar energy transfer rate on the lateral chain length.

3. Analysis of the Excited States

In this section we report first the properties of the isolated chromophore (section 3.1) and then those of the columnar aggregates (section 3.2). Our experimental results have shown that the lateral chain length does not significantly affect the spectroscopic properties. For this reason and in order to reduce the computing time into reasonable limits, the theoretical calculations have been carried out for H1T.

3.1. Isolated Chromophore. After a brief description of the procedure (section 3.1.1), we show the properties of the first four singlet excited states (section 3.1.2). We also give a representation of the electronic density of H1T at a molecular level for its ground state and the excited states S_1 and S_4 (section 3.1.3). Such a representation is necessary for the determination of the intermolecular interactions (section 3.2).

3.1.1. Procedure. Molecular orbital calculations were carried out using the CS-INDO method described in detail elsewhere.³³ The INDO parameters (screening factors for the resonance integrals and one-center and two-center integrals) were taken from ref 34. The structural parameters of H1T used for the calculations are given in Figure 6. These values are deduced from the results obtained by X-ray diffraction on triphenylene crystals³⁵ which are averaged so that a D_{3h} symmetry is obtained for the aromatic core. The six methoxy groups were assumed to be identical.³⁶ Their orientation with respect to the aromatic core is not fixed, since free rotation may take place. Calculations carried out for *o*-dimethoxybenzene have shown that the orientation of the substituents is the result of two antagonistic effects: conjugation of the oxygen lone pair with the aromatic ring favors conformations where the O—C bonds of the methoxy

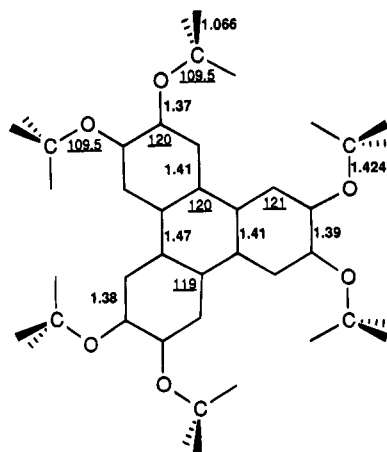


Figure 6. Structural parameters of H1T used for quantum chemistry calculations. Bold and underlined numbers represent respectively bond lengths (in Å) and angles (in deg).

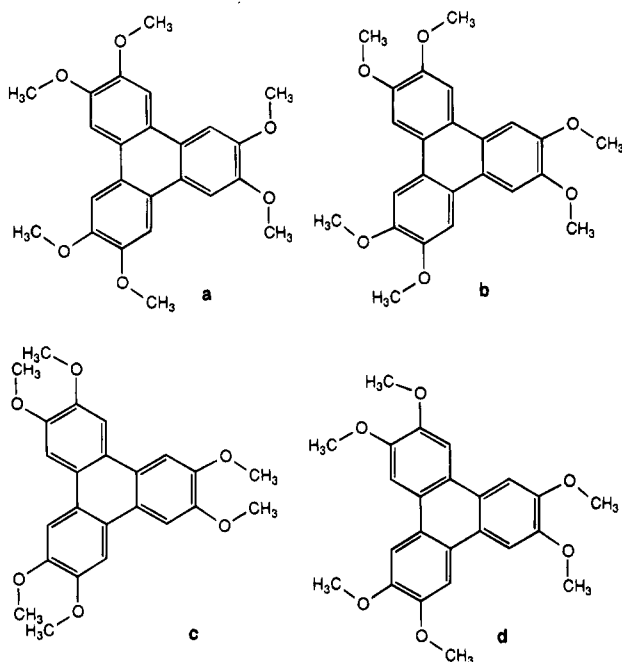


Figure 7. Schematic representation of the planar conformers of H1T having a threefold symmetry axis (a–c) and of one planar conformer with lower symmetry (d).

are coplanar with the phenyl group while repulsion between the hydrogens of OCH₃ and the hydrogen of the aromatic ring at the ortho position favors nonplanar conformations.³⁷ NMR studies revealed that planar conformations are predominant in solution³⁸ whereas in the gas phase out of plane conformations are observed.³⁹ Temperature dependent NMR experiments performed for the liquid crystalline phase of H6T suggest that the O–C bonds of the alkyloxy chains are most probably coplanar with the aromatic core.⁴⁰ For this reason, in the present work, we consider planar conformations. In this case, several planar conformers are possible depending on the relative orientation of two neighboring methoxy groups. Figure 7 shows the conformers characterized by a threefold symmetry axis (a–c) and one with lower symmetry (d).

At first, configuration interaction (CI) calculations taking into account all the singly excited configurations built on the 45 highest occupied and the 25 lowest virtual molecular orbitals (MOs) were performed. Further calculations considering singly, doubly, and triply excited configurations in the space of the most important π MO (six occupied and six unoccupied) were

also made. A second-order perturbation treatment⁴⁰ was not carried out because of the large size of the chromophores.

3.1.2. Excited States. Table 2 shows the properties of the four lowest singlet-singlet transitions of H1T having a D_{3h} symmetry. All the examined transitions are polarized within the aromatic plane. The transitions $S_0 \rightarrow S_1$ and $S_0 \rightarrow S_2$ are symmetry forbidden while both $S_0 \rightarrow S_3$ and $S_0 \rightarrow S_4$ are allowed and degenerate. Rotation of the methoxy groups is expected to affect only slightly the properties of those transitions because they involve only π orbitals of the aromatic core. Indeed, for the planar conformer **d**, the transition $S_0 \rightarrow S_1$ which is no more symmetry forbidden is characterized by a weak transition moment (0.3 D). For the same reason, the electronic transitions of H1T are expected to have the same symmetry as those of the unsubstituted triphenylene. Our results obtained with doubly and triply excited configurations are in agreement with results reported in the literature.⁴² It is worth-noticing that CI with singly excited configurations yield roughly the same properties except the symmetry of the two lowest transitions. In both cases, the most intense transition is the $S_0 \rightarrow S_4$.

The calculated energy (28 500 cm⁻¹) of the $S_0 \rightarrow S_1$ transition is close to the experimental value (27 700 cm⁻¹) but the experimentally found transition moment (0.9 D) is higher than the calculated one for rotamer **d** (0.3 D). This is not surprising since, on the one hand, various rotamers may exist in solution, and on the other, our calculations do not take into account the vibrational coupling usually reinforcing the oscillator strength. The overestimation of the $S_0 \rightarrow S_4$ transition energy is probably due to the fact that reorganization of the σ system accompanying a $\pi \rightarrow \pi^*$ excitation is neglected. Such a reorganization should lower the energy of the higher excited states.

3.1.3. Representation of the Electronic Density. The electronic density can be represented by a multipolar distribution (charge, dipole, quadrupole, ...) located on each atom. As a first step, we calculate the net charge borne by each atom in the ground state, which is found to be small (Figure 8a). Moreover, Figure 8b shows that the $S_0 \rightarrow S_4$ electronic transition induces only a small charge transfer obeying the D_{3h} symmetry. The charge transfer induced by the $S_0 \rightarrow S_1$ transition is even smaller: the maximum charge difference per atom is 0.01 e.

The above findings (small net charge borne by each atom and small charge transfer induced by the electronic transitions) lead to the conclusion that the representation of the electronic density only by a charge per atom may be a poor approximation for the determination of the electrostatic intermolecular interactions. In order to improve this representation we determine both the net atomic charge and a dipole on each atom X. The definition of this dipole originates from the definition of the total molecular dipole, μ , sum of the electronic and nuclear molecular dipoles (μ_e and μ_N).

$$\mu_e = \langle |\phi_1 \phi_2 \phi_3 \dots \phi_n| | \sum_{\text{electrons}} \mathbf{R}_e | | \phi_1 \phi_2 \phi_3 \dots \phi_n \rangle \quad (1)$$

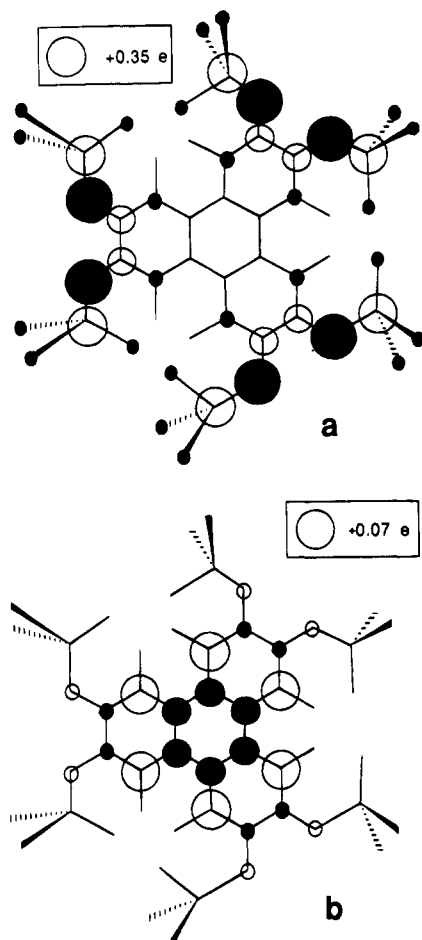
For the ground state, $|\phi_1 \phi_2 \phi_3 \dots \phi_n|$ is the self-consistent field (SCF) wave function in which each molecular orbital ϕ_i can be written as a linear combination of the atomic orbitals (AO) χ_p .

$$\phi_i = \sum_{\text{AO}_p} c_i^p \chi_p \quad (2)$$

\mathbf{R}_e is the mono-electronic displacement operator centered at a fixed point of the molecule. Within the frame of the INDO approximation (only the monocentric integrals $\langle \chi_p | \mathbf{R}_e | \chi_q \rangle$ may be different from zero), we get

TABLE 2: Properties of the Four Lowest Electronic Singlet Transitions of H1T (Conformer a Characterized by D_{3h} Symmetry; Figure 7) with μ the Transition Moment

transition	CI with singly excited configurations			CI with singly, doubly, and triply excited configurations			exp values	
	symmetry	energy, cm^{-1}	μ (xy, z), D	symmetry	energy, cm^{-1}	μ (xy, z), D	energy, cm^{-1}	μ (xy, z), D
$S_0 \rightarrow S_1$	A_2'	30 600	(0, 0)	A_1'	28 500	(0, 0)	27 700	(0.9, 0)
$S_0 \rightarrow S_2$	A_1'	31 400	(0, 0)	A_2'	33 200	(0, 0)	ca. 30 300	
$S_0 \rightarrow S_3$	E'	37 000	(3.0, 0)	E'	34 200	(1.3, 0)	32 400	(ca. 4.5, 0)
$S_0 \rightarrow S_4$	E'	39 000	(5.2, 0)	E'	40 200	(7.3, 0)	36 000	(ca. 10, 0)

**Figure 8.** Net charge borne by each atom of H1T in its ground state (a) and charge transfer induced by the $S_0 \rightarrow S_4$ transition (b). Black and white disks represent respectively negative and positive charge attributed to each atom. The disk area is proportional to the absolute charge.

$$\mu_e = 2 \sum_{i=1,n} \langle \phi_i | \mathbf{R}_e | \phi_i \rangle = 2 \sum_{i=1,n} \sum_{AO_p \in X} c_i^p \sum_{AO_q \in X} c_i^q \langle \chi_p | \mathbf{R}_e | \chi_q \rangle \quad (3)$$

The mono-electronic operator \mathbf{R}_e may be separated into two components: the first one \mathbf{R}_e^X depends only on the position of the atom X while the second \mathbf{r}_e yields the position of the considered electron with respect to the position of the atom X.

$$\mu_e = 2 \sum_{\text{atomsX}} \left\{ \sum_{AO_p \in X} \sum_{AO_q \in X} \langle \chi_p | \mathbf{R}_e^X | \chi_q \rangle + \langle \chi_p | \mathbf{r}_e | \chi_q \rangle \right\} \left(\sum_{i=1,n} c_i^p c_i^q \right) \quad (4)$$

Equation 4 shows that μ_e can be expressed by a summation on all the atoms of the molecule.

$$\mu_e = \sum_{\text{atomsX}} \mu_e^X \quad (5)$$

with

$$\mu_e^X = 2 \left\{ \sum_{AO_p \in X} \sum_{AO_q \in X} \langle \chi_p | \mathbf{R}_e^X | \chi_q \rangle + \langle \chi_p | \mathbf{r}_e | \chi_q \rangle \right\} \left(\sum_{i=1,n} c_i^p c_i^q \right) \quad (6)$$

Since \mathbf{R}_e^X does not depend on the position of the electron, the term $\langle \chi_p | \mathbf{R}_e^X | \chi_q \rangle$ is different from zero only if the atomic orbitals χ_p and χ_q are identical. Thus eq 6 can be rewritten as the following:

$$\mu_e^X = \left(2 \sum_{AO_p \in X} \sum_{OMO_i} c_i^p{}^2 \right) \mathbf{R}_e^X + \text{electronic charge contribution } (Q_e^X \mathbf{R}_e^X) + 2 \sum_{AO_p \in X} \sum_{AO_q \in X, q \neq p} \langle \chi_p | \mathbf{r}_e | \chi_q \rangle \sum_{i=1,n} c_i^p c_i^q \quad (7)$$

elementary dipole (λ^X)

If we take into account the nuclear charge Q_N^X , the total atomic dipole μ^X can be expressed as

$$\mu^X = (Q_N^X - Q_e^X) \mathbf{R}_e^X + \lambda^X \quad (8)$$

So in the multipolar multicentric development, a charge ($Q_N^X - Q_e^X$) and an elementary dipole λ^X are attributed to each atom. One can understand that it is crucial to take into account charge-dipole and dipole-dipole interactions in the evaluation of the electrostatic interactions between two molecules. For instance, the charge-charge terms represent only a third of the electrostatic interaction between two parallel and coaxial molecules of H1T separated by 3.6 Å. These remarks concerning the evaluation of electrostatic interactions in a H1T dimer also concern interactions between molecules possessing a permanent dipole moment. However, in the specific case of ionic chromophores,¹⁷ the multipolar multicentric development can be limited to only a net charge per atom, since the charge-charge terms are predominant in the electrostatic interaction.

In the case of an excited state, the same formal development can be made by using natural orbitals and their occupation numbers obtained by diagonalization of the first-order density matrix.

3.2. Columnar Aggregates. Our study is focused in columnar stacks formed by ten H1T molecules. Information concerning the arrangement of the aromatic cores is provided by X-ray diffraction measurements:¹⁶ the stacking distance is 3.6 Å, and the aromatic cores are centered and perpendicular to the column axis. Concerning the relative orientation of molecular disks within the stacks, we have considered an helicoidal geometry. The angle between two neighboring molecules is 33°. Since such a helicoidal geometry has only a short coherence length, we have also examined stacks in which two neighboring molecules are at a relative angle of either +33° or -33°; these two angle values are randomly distributed along the columnar aggregate. Moreover, in order to get some insight

into the role played by the structural defects, we study the variation of the diagonal and off-diagonal terms in the matrix Hamiltonian corresponding to a dimer formed by two parallel and coaxial HIT molecules as a function of their stacking distance and their relative orientation.

The general methodology used in this part of our work is described in detail in ref 17. In section 3.2.1 we briefly describe the successive stages of investigation followed in the analysis of the excited states of columnar aggregates. In section 3.2.2 we present the formalism we developed for the calculation of the coupling between transition moments. Finally, the results of our calculations are shown in section 3.2.3.

3.2.1. General Methodology. The excited states of aggregates are calculated as a linear combination of the excited states localized on each chromophore of the system (excitonic theory).⁴⁴⁻⁴⁶ The original point of this methodology consists of the calculation of the diagonal and off-diagonal terms of the Hamiltonian matrix, taking into account the structure and charge distribution of each molecule and the precise geometry of the aggregate.

The diagonal terms represent the excitation energy of each chromophore within the aggregate. In the manner of solvent molecules, the nonexcited molecules of the aggregate may stabilize in a different way the ground state and the excited state of the considered excited chromophore. Thus, the excitation energy may be different from that of the isolated molecule and differ from one site to the other. In order to determine the energetic topography of the aggregate, i.e. the excitation energy for each site of the aggregate, we calculate the difference between two interaction energies: (i) the interaction energy between the examined chromophore in its ground state and the other molecules of the aggregate and (ii) the interaction energy between the examined chromophore in its excited state and the other molecules of the aggregate. The intermolecular interactions are evaluated using the semiempirical Claverie's model, according to which the interaction energy is expressed as a sum of the electrostatic, polarization, dispersion, and repulsion energies, all calculated by analytical expressions.⁴⁷ Electrostatic and polarization terms are calculated by using the net charges and the elementary dipoles as previously defined.

The off-diagonal terms represent the interaction between transition moments. This interaction can be approximated by the interaction between the two electronic transition dipoles. However, such an approximation is inappropriate when the interchromophore distance is short compared to the molecular dimensions. The extended dipole approximation providing a better approach for certain systems⁴⁸ has been used in the case of columnar aggregates of ionic compounds.¹⁷ In the present work, we perform a direct quantum mechanical calculation without any further approximations than those of the INDO formalism.

3.2.2. Interaction between Transition Moments. After CI of the monoexcited configurations, the wave function of the chromophore m in its S_a electronic excited state is expressed as a linear combination of all the monoexcited configurations:

$$|m_a\rangle = \sum_{\text{conf}(i_m, j_m)} A_{i_m, j_m} (\phi_{i_m}^m \rightarrow \phi_{j_m}^m) \quad (9)$$

where $\phi_{i_m}^m$ represents an occupied MO and $\phi_{j_m}^m$ a virtual MO of the molecule m . In the same way, the wave function of the chromophore n in the S_b electronic excited state is expressed as:

$$|n_b\rangle = \sum_{\text{conf}(i_n, j_n)} B_{i_n, j_n} (\phi_{i_n}^n \rightarrow \phi_{j_n}^n) \quad (10)$$

where the SCF molecular orbitals ϕ are linear combinations of the atomic orbitals χ :

$$\phi_{i_m}^m = \sum_{\text{AO}_p} c_{i_m, p}^p \chi_p^m \quad (11)$$

The coupling between the two transition moments is the matrix element of the dimer Hamiltonian $\langle m_a n_0 | \mathcal{A} | m_0 n_b \rangle$, where the dimer wave functions $m_a n_0$ and $m_0 n_b$ correspond to the excitation of the chromophore m in its S_a state and to the excitation of the chromophore n in its S_b state, respectively. Since both wave functions differ by two molecular orbitals, only the bielectronic part of the Hamiltonian has a contribution to the coupling:

$$\langle m_a n_0 | \mathcal{A} | m_0 n_b \rangle = \sum_{(i_m, j_m)} \sum_{(i_n, j_n)} A_{i_m, j_m} B_{i_n, j_n} (2(\phi_{i_m}^m \phi_{j_m}^m, \phi_{i_n}^n \phi_{j_n}^n) - \text{dipolar term} \\ (\phi_{i_m}^m \phi_{i_n}^n, \phi_{j_m}^m \phi_{j_n}^n)) \quad (12) \\ \text{exchange term}$$

with the following definition of the bielectronic integrals:

$$(\phi^i \phi^j, \phi^k \phi^l) = \int \int \phi^i(1) \phi^j(1) \frac{1}{r_{12}} \phi^k(2) \phi^l(2) d\tau_1 d\tau_2 \quad (13)$$

In the INDO formalism, the exchange term is equal to zero and the coupling between the two transition moments can be written as a linear combination of bicentric bielectronic integrals whose calculation is very easy:

$$\langle m_a n_0 | \mathcal{A} | m_0 n_b \rangle = 2 \sum_{\text{AO}_p \in m} \sum_{\text{AO}_q \in n} (\chi_p^m \chi_p^m, \chi_q^n \chi_q^n) \times \\ \sum_{(i_m, j_m)} \sum_{(i_n, j_n)} A_{i_m, j_m} B_{i_n, j_n} c_{i_m}^p c_{j_m}^p c_{i_n}^q c_{j_n}^q \quad (14)$$

In the above treatment, only the monoexcited configurations have to be considered because the contribution of the multiexcited configurations to the coupling is equal to zero (matrix elements between wave functions differing by more than two molecular orbitals).

The present formalism (eqs 8-13) is an important improvement in the determination of the interaction between electronic transition moments, in particular when the transition is weak. The term $\langle m_a n_0 |$ represents an electronic density associated with the transition $S_0 \rightarrow S_a$ (respectively $|m_0 n_b\rangle$ for $S_0 \rightarrow S_b$). In the same way as for the electronic density of an electronic state section 3.1.3, the electronic density associated to a given transition can be represented by a multipolar multicentric development. Then the matrix element $\langle m_a n_0 | \mathcal{A} | m_0 n_b \rangle$ corresponds to the electrostatic interaction between two charge distributions derived from the wave functions of the ground and the excited states using an infinite multipolar multicentric development (charge, dipole, quadrupole, ... on each atom). The direct quantum mechanical calculation method we propose here takes into account the charge-charge, charge-dipole, dipole-dipole, dipole-quadrupole, ... interaction terms between all the atoms of the chromophore m and those of the chromophore n . These terms vary respectively as $1/R$, $1/R^2$, $1/R^3$, $1/R^4$, ... with the distance R between pairs of atoms. The coupling calculated according to the extended dipole approximation model is only the sum of four charge-charge electrostatic interactions.⁴⁸ Therefore, in the extended dipole model, the coupling V

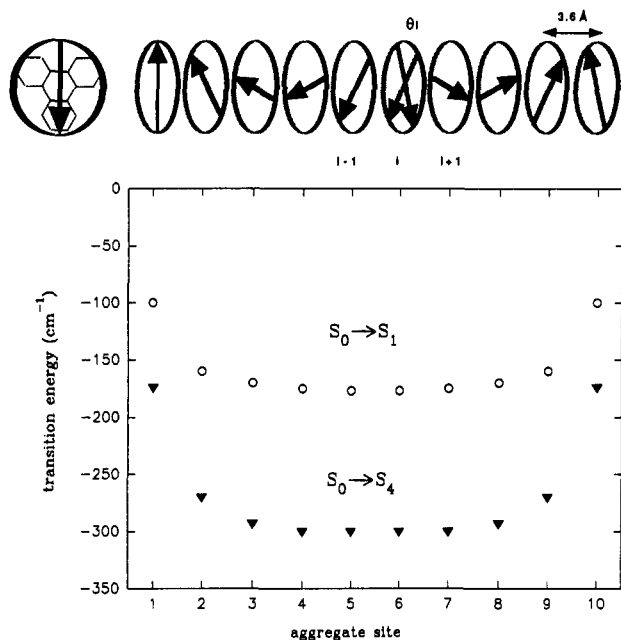


Figure 9. Energetic topography of a helicoidal H1T decamer corresponding to the $S_0 \rightarrow S_1$ (a) and the $S_0 \rightarrow S_4$ (b) transitions. The geometry of the H1T stacks used in the calculation is shown at the top; the angle θ_i formed between two neighboring molecules is $\pm 33^\circ$.

decreases at long distances as a dipole–dipole interaction ($1/R^3$) while, at short distances, it decreases as a charge–charge interaction ($1/R$) so that

$$\lim_{R \rightarrow 0} VR^3 = 0$$

A monocentric multipolar development is considered in a recent publication dealing with the coupling in a naphthalene dimer.⁴⁹ In that paper, the transition moment is assimilated to a dipole, quadrupole, octopole, ... located on the center of the molecule (and not on each atom as in the present work) and it is shown that higher order terms (dipole–octopole, octopole–octopole, ...) have an important contribution in the electronic coupling.

3.2.3. Results and Discussion. Figure 9 shows the energetic topography of a helicoidal columnar stack formed by ten H1T molecules for the $S_0 \rightarrow S_1$ and $S_0 \rightarrow S_4$ transitions. It illustrates the perturbation of the transition energies of each chromophore due to its environment. We can make two main remarks. (I) Edge effects are observed but the difference in the excitation energy between edge and central sites and the difference between the excitation energies of the isolated molecule and the molecules within the aggregates are smaller than 70 and 130 cm⁻¹ for $S_0 \rightarrow S_1$ and $S_0 \rightarrow S_4$, respectively. In the temperature domain in which the H1T mesophases are thermodynamically stable, the Boltzmann factor is *ca.* 250 cm⁻¹. Therefore, at these temperatures, all the molecules of the stack are expected to have the same excitation energy. (II) In spite of the non-centrosymmetric geometry of the aggregate, its energetic topography is completely symmetric. Moreover, we have found that the topography does not depend on the relative orientation of the molecules within the columnar stack.

These remarks show that the energetic topography of the H1T stacks has completely different features than that of the stacks formed by triaryl pyrylium salts.¹⁷ In the latter case, the excitation energy is very different from that of the isolated chromophores and it is quite sensitive to the chromophore orientation around the column axis. Such a difference is due to the fact that the charge transfer induced by the examined electronic transitions is very big for triaryl pyrylium cations

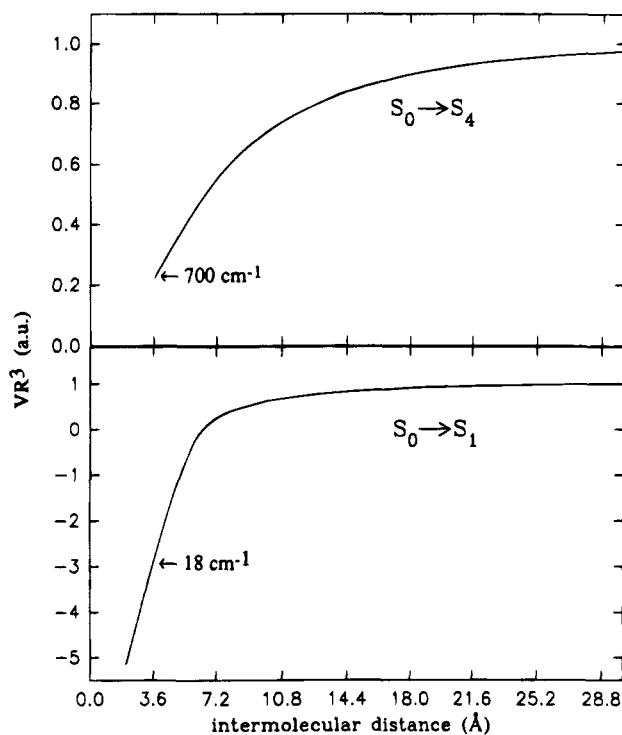


Figure 10. Distance dependence of the interaction energy between two transition moments V of two parallel and coaxial H1T molecules with a relative 33° angle between them. The arrows denote the coupling at 3.6 Å corresponding to the stacking distance in the columnar mesophases of H1T.

while it is very weak for H1T (section 3.1.3). The weak charge transfer in the hexakis(alkyloxy)triphenylenes has a further consequence: the perturbation of the excitation energy induced by structural defects in the mesophase will be smaller than the Boltzmann factor corresponding to the temperature domain of the H1T liquid crystals, and therefore, all the molecules will be energetically equivalent. The above finding of our theoretical calculations is in agreement with the time-resolved fluorescence spectra of the H1T mesophases recorded following laser excitation. Indeed, when the time window of the observation is varied, no spectral diffusion of the fluorescence is observed. Contrary to H1T mesophases, columnar liquid crystals of triaryl pyrylium salts show strong spectral diffusion of the fluorescence.¹⁸

We have calculated the interaction V between the transition moments of two coaxial and parallel H1T molecules. We have considered the conformer **d** and not the conformers characterized by a threefold symmetry axis because the latter have zero oscillator strength for the two lowest singlet transitions. Figure 10 shows the variation of V as a function of the stacking distance R for $S_0 \rightarrow S_4$ and $S_0 \rightarrow S_1$. At long distances ($R > 25$ Å), the well-known $1/R^3$ dependence is found for both transitions. Conversely, at short distances, the coupling is quite different from what is predicted by the dipole–dipole model. Moreover, at short distances the interactions corresponding to $S_0 \rightarrow S_4$ and $S_0 \rightarrow S_1$ exhibit different behaviors.

The $S_0 \rightarrow S_4$ transition has a strong dipole moment (5.3 D), and therefore, the first two terms of the multipolar development (charge and dipole) attributed to each atom are expected to play a predominant role in the estimation of the coupling, even at relatively short distances. Indeed, we have found that, at distances of 3–4 Å, the coupling is equivalent to a charge–charge interaction ($1/R$ dependence). In this case, the extended dipole model provides a good evaluation of the coupling. $S_0 \rightarrow S_3$ shows exactly the same behavior as $S_0 \rightarrow S_4$.

Conversely to $S_0 \rightarrow S_4$ and $S_0 \rightarrow S_3$, $S_0 \rightarrow S_2$ and $S_0 \rightarrow S_1$ are weak dipolar transitions having transition moments 0.4 and 0.3 D, respectively. Consequently, the other terms (quadrupole, octopole, ...) in the multipolar development cannot be neglected in the calculation of the interaction at short distances. For $S_0 \rightarrow S_1$, we have found that, at 3–4 Å, the coupling is equivalent to a quadrupole–quadrupole or dipole–octopole ($1/R^5$ dependence). In the case of $S_0 \rightarrow S_2$, a charge–dipole term seems ($1/R^2$ dependence) to be important. This means that the extended dipole model is not valid for those weak transitions. We should emphasize that the present statement concerns only the electronic coupling of the conformer **d**.

The curve shown in Figure 10 can be fitted with the empirical formula:

$$VR^3 = C[1 - \exp(-aR^b)] \cos \theta \quad (15)$$

where $a = 0.07$, $b = 1.18$, and C is a constant. Equation 15 is approximately valid for all relative orientations of the molecules in the dimer for both $S_0 \rightarrow S_4$ and $S_0 \rightarrow S_3$. We must stress that the distance dependence of the coupling calculated for $S_0 \rightarrow S_2$ is not the same as that calculated for $S_0 \rightarrow S_1$. Moreover, for those transitions, a strong dependence of the coupling with the angle θ , not proportional to $\cos \theta$, is found. Consequently, it has not been possible to deduce a simple analytical formula as in eq 15.

Figure 10 shows that, at 3.6 Å, which is the distance between two neighboring molecules in the mesophases, the coupling V is 700 and 18 cm^{-1} for $S_0 \rightarrow S_4$ and $S_0 \rightarrow S_1$, respectively. In the first case, V is larger than the Boltzmann factor (250 cm^{-1}), while in the latter it is smaller. Consequently, coherent excitations are expected for $S_0 \rightarrow S_4$, and localized ones, for $S_0 \rightarrow S_1$.

We have calculated the properties of the eigenstates of a H1T decamer corresponding to the transition $S_0 \rightarrow S_4$. $S_0 \rightarrow S_4$ is a degenerate transition, and therefore, its two components, polarized in the plane of the triphenylene core and orthogonal to each other, are taken into account as two independent transitions in the excitonic matrix. Moreover, we take into account all the off-diagonal terms and not only those corresponding to nearest neighbors. We have considered both a helicoidal geometry and that of randomly oriented disks ($\theta_i = \pm 33^\circ$; Figure 9). In both cases we have found that the oscillator strength mainly arises from the two upper eigenstates which are degenerate; the lower eigenstates have very low but non-zero oscillator strength ($f < 0.001$). The shift of the absorption maximum with respect to the corresponding peak of the isolated molecule is 1364 and 1377 cm^{-1} , respectively, for the helicoidal stack and the stack with randomly oriented molecules. These values are of the same order of magnitude as the experimentally determined shift ($2000 \pm 500 \text{ cm}^{-1}$; Figure 3).

Finally, it is interesting to compare the values of the coupling calculated through quantum mechanical calculations for the conformer **d** of H1T to some experimental evaluation. It is possible to obtain such an evaluation by comparing the absorption spectrum of H5T solutions to that of its mesophase (Figure 3). Knowing that the excitonic shift ΔE is twice the coupling, we deduce that $V(S_0 \rightarrow S_4) = 1000 \pm 250 \text{ cm}^{-1}$. Moreover, considering that the transition moment of $S_0 \rightarrow S_1$ is about ten times smaller than that of $S_0 \rightarrow S_4$ (Table 2) and that the coupling is proportional to the square of the transition moment (dipolar interactions), we have $V(S_0 \rightarrow S_1) = 10 \text{ cm}^{-1}$. The values of both $V(S_0 \rightarrow S_4)$ and $V(S_0 \rightarrow S_1)$ are of the same order of magnitude as those determined theoretically (700 and 18 cm^{-1}).

4. Monte Carlo Simulations

We have seen in the previous section that, for two neighboring molecules in the HnT mesophases, the coupling corresponding to the $S_0 \rightarrow S_1$ transition (experimental value, 10 cm^{-1} ; theoretical value, 18 cm^{-1}) is much weaker than the Boltzmann factor (250 cm^{-1} at 80 °C). Therefore, it is reasonable to model excitation transfer on the basis of a hopping mechanism.

In this section we present first the general procedure followed in the Monte Carlo simulations (section 4.1). We discuss the distance and angle dependence of the hopping probability (section 4.2), which determines the temporal and spatial evolution of the excitation in the columnar mesophases. In section 4.3 we show the values of the hopping time obtained by fitting the experimental decay curves with the simulated ones using various models; the coupling deduced from the hopping time is compared to the coupling determined in section 3.

4.1. General Procedure. The fluorescence decay curves are simulated by calculating the survival probability of the excitation characterized by a lifetime τ_f and performing a random walk on a three-dimensional lattice containing traps.

The lattice consists of 10^6 sites and has the main geometrical features of the columnar mesophases. In the z direction, the sites are at a distance of 3.6 Å and their number, corresponding to the column length, is varied from 50 to 3000. In the xy plane the sites form a hexagonal lattice, the distance between neighboring sites being 20.2, 22.6, and 24.3 Å, corresponding to H5T, H7T, and H9T, respectively.

The sites are designated as hosts (HnT molecules) or traps (TNF molecules). The traps are always in much lower concentration than the host sites, and they are randomly distributed among the hosts. For the calculation of each simulated decay, the trap concentration is given the value $x_{\text{tr}} = x_{\text{TNF}} + x_{\text{intr}}$, where x_{TNF} and x_{intr} are respectively the TNF and the intrinsic trap concentration of the corresponding experimental decay. On the basis of our experimental observations, x_{intr} is taken to be equal to 10^{-3} .

The “particles”, corresponding to excitations localized on individual molecules, are randomly placed on the lattice, and they hop from site to site according to the following pattern. Along the z direction, long-distance hops until the eighth neighbor (eight above and eight below) may take place. In the xy plane only hops to the six nearest neighbors (nearest columns) are allowed. For intercolumnar jumps, the particle also may hop in the z direction eight sites above or eight sites below its initial xy plane. Cyclic boundary conditions are used in the x and y directions; in the z direction, both cyclic boundary and reflecting boundary conditions are realized. The hopping probability to a distance R is given by a function $p_z(R)$ for sites located in the same column and by $p_{xy}(R)$ for sites located in neighboring columns. When a particle reaches a trap site, its motion stops.

The total number of steps made by one “particle” is recorded. This is considered as one run. A large number of independent runs is performed, typically 10^5 . In this way we obtain a histogram of all runs, yielding the survival probability. The abscissa corresponds to the number of steps, and the ordinate, to the number of runs that did not result in trapping (survived “particles”) at each step. By using the hopping time t_h , *i.e.* the reciprocal of hopping frequency, as a fitting parameter, we can convert the number of steps to real time. Then, this curve is convoluted with the instrumental response function and multiplied by $\exp(-t/\tau_f)$. Practically t_h is varied in order to obtain a good fitting between the experimental and the simulated decay curves.

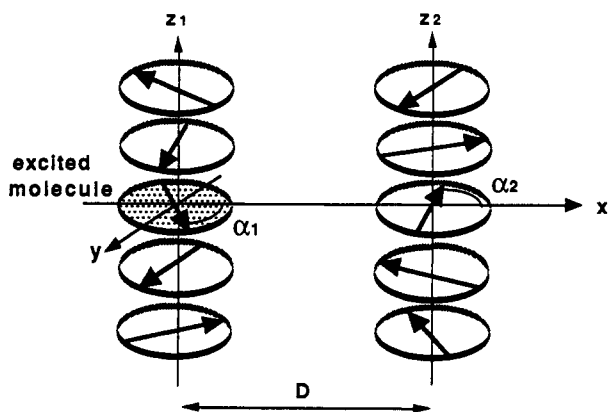


Figure 11. Illustration of the angles between transition moments involved in intercolumnar hops.

The fluorescence lifetime used in the simulations is 12.4 ns, determined for H6T in a liquid crystalline solvent.⁶

4.2. Probability of Hopping. A crucial point in the present analysis is the definition of the functions $p_z(R)$ and $p_{xy}(R)$. The probability of hopping is proportional to the square of the interaction energy between transition moments. Our quantum chemical calculations have shown that the distance and angle dependence of the coupling greatly depends on the strength of the transition (section 3.2.2). The $S_0 \rightarrow S_1$ transition moment experimentally determined for HnT (0.9 D), although weak, is three times bigger than that calculated (0.3 D) for conformer **d** (Figure 5). Consequently, the calculated distance and angle dependence of the coupling may not be realistic. For this reason, we test four different models, three of them corresponding to dipolar interactions between nearest neighbors while the fourth one corresponds to multipolar interactions.

As a first approximation, widely used in energy transfer studies, we consider a $1/R^6$ dependence for the hopping probability, leading to $p_z(R) = p_{xy}(R) = K/R^6$, where K is a constant. In this approximation, molecules are assimilated to simple points on the lattice.

At a second step, we maintain the same distance dependence but we take into account the relative orientation of the transition moments. Now the molecules correspond to vectors located on the lattice sites. In this case, the hopping probability between two sites within the same column is equal to $(K/R^6)(\cos \alpha)^2$, where α is the angle between the corresponding transition moments. It must be stressed that, for the $S_0 \rightarrow S_1$ transition, the angle α is not the same as the angle θ formed between two neighbouring molecules as defined in Figure 9. One reason is that the polarization of this weak electronic transition depends on the conformation of the six alkyloxy groups. Secondly, the electronic coupling involves vibronic modes which have various orientations. Therefore, we have considered that the transition moments are randomly distributed around the column axis. Consequently, the fitting parameter τ_h corresponds to an average value of the hopping probability to the nearest neighbor in the same column: $p_z(R) = K/2R^6$. In order to determine $p_{xy}(R)$, we must take into account the fact that there is no correlation between the orientation of the chromophores located in different columns. Knowing that the coupling between two coplanar transition moments is given by the formula:⁵⁰

$$V(R, \alpha_1, \alpha_2) = \frac{\sqrt{K}}{R^3} (2 \cos \alpha_1 \cos \alpha_2 - \sin \alpha_1 \sin \alpha_2) \quad (16)$$

where the angles α_1 and α_2 are defined in Figure 11; the intercolumnar hopping probability in the xy plane is

$$p(R, \alpha_1, \alpha_2) = \frac{K(2 \cos \alpha_1 \cos \alpha_2 - \sin \alpha_1 \sin \alpha_2)^2}{R^6} \quad (17)$$

By taking the average of $p(R, \alpha_1, \alpha_2)$ over all the angles α_1 and α_2 , we find:

$$p_{xy}(R) = \frac{7}{4} \frac{K}{R^6} \quad (18)$$

Since $d \ll D$, we can assume that eq 18, derived for coplanar chromophores, is approximately valid for intercolumnar hopping to molecules located not too far from the xy plane Figure 11.

In a third series of simulations, we assume that the extended dipole approximation is valid. Then, using eq 15 and taking into account the chromophore orientation as described above, we have $p_z(R) = K[1 - \exp(-aR^b)]^2/2R^6$ and $p_{xy}(R) = 7K[1 - \exp(-aR^b)]^2/4R^6$.

Finally, in order to simulate strong nearest neighbor coupling in which multipolar interactions are predominant, we take $p_z(R) = K/2R^{10}$; for intercolumnar hops dipolar interactions are considered ($p_{xy}(R) = 7K/4R^6$).

4.3. Results and Discussion. All the experimental fluorescence decay curves can be fitted relatively well with the simulated ones when the hopping probability used in the calculations corresponds to dipolar interactions, either according to the oversimplified pattern or to the more sophisticated ones (Figures 12 and 13). Conversely, it is impossible to obtain any acceptable fit for multipolar intracolumnar interactions ($p_z(R) = K/2R^{10}$) and dipolar intercolumnar ones ($p_{xy}(R) = 7K/4R^6$); in this case the simulated curves decay always more rapidly than the experimental ones.

Tables 3–5 show the values of the hopping time, giving the best fit for the three models corresponding to dipolar interactions. We can remark that the more simplified the model used the smaller the hopping time determined through the fitting procedure. Thus, if the molecules are considered as simple points on a three-dimensional lattice, the hopping time values are found to be more than 1 order of magnitude smaller (Table 3) than those determined by taking into account molecular orientation and molecular dimensions (Table 5).

We have also checked the influence of the column length (number of sites in the z axis) used in the simulations on the determined value of the hopping time. Figure 14 shows that the shorter the column length, the smaller the value, yielding the best fit between experimental and simulated decay curves. This dependence reaches a plateau when more than 500 sites are considered in the z direction. In the HnT mesophases the column length is polydisperse. It depends on the heat treatment and most probably differs from one sample to the other. The fact that the experimental decays are reproducible indicates that the number of molecules involved in the energy transfer process per column is at least 500.

Another interesting remark concerns the difference in the hopping time determined for H5T, H7T, and H9T: the longer the lateral chain lengths, the bigger the hopping time. This dependence is true for all three pairs of $p_z(R)$ and $p_{xy}(R)$ functions used and cannot be due to a variation of the column length. A similar result has been reported previously for the triplet transfer in the liquid crystalline phases of metal-free phthalocyanines: the hopping time was found to be 7.4 or 66 ps when the macrocycles are substituted by eight dodecyl or eight octadecyl chains, respectively, indicating that when the liquid part of the material increases, the energy transfer becomes less efficient.¹¹ However, such a statement must be considered

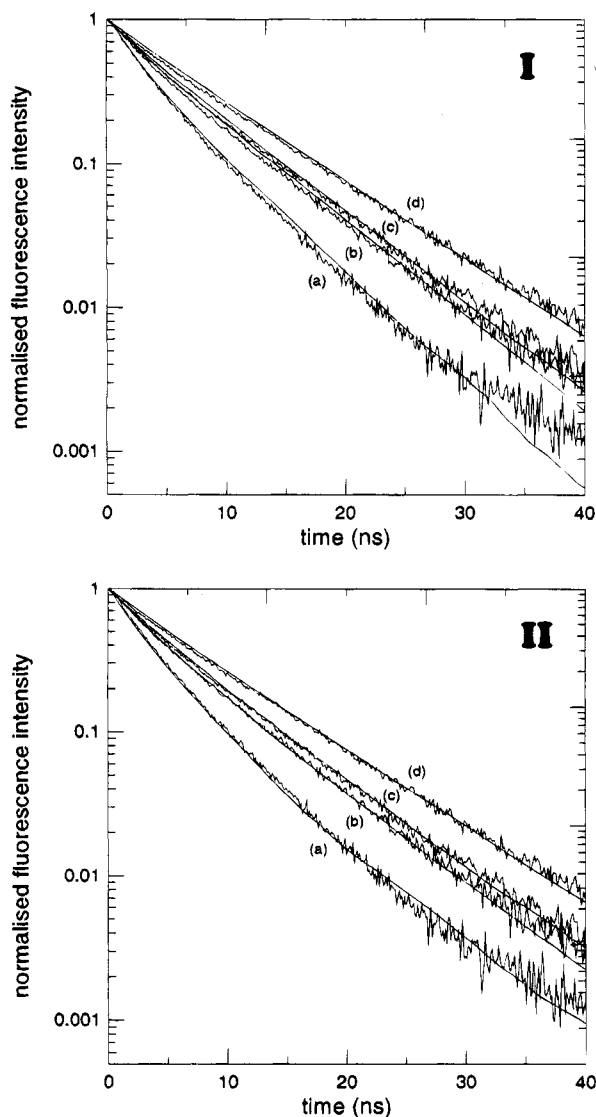


Figure 12. Fitting of experimental fluorescence decays recorded for the H5T mesophases with the simulated ones. Experimental conditions: TNF molar fraction (a) 5×10^{-3} , (b) 2×10^{-3} , (c) 10^{-3} , (d) 0; $\lambda_{\text{ex}} = 295$ nm; $\lambda_{\text{em}} = 400$ nm; $T = 80$ °C. Simulation parameters: fluorescence lifetime, 12.4 ns; intrinsic trap concentration, 10^{-3} ; column length, 1000 sites; hopping probability, varies with the distance as (I) $p_z(R) = p_{xy}(R) = 1/R^6$ or (II) $p_z(R) = K/2R^6$ and $p_{xy}(R) = 7K/4R^6$. The experimental curves are the noisy ones.

with caution. As a matter of fact, the lattice used in the simulations is static while real systems are not. Lateral diffusion of the chromophores in the H5T mesophases occurs even in the nanosecond time scale.⁴⁰ When the length of the six side chains increases, molecular motion is expected to become slower. This could explain why the fits obtained for H7T and H9T are better than those of H5T (Figure 13).

The hopping time determined by means of Monte Carlo simulations corresponds to a hopping frequency $1/t_h$, which is related to the coupling V through Fermi's golden rule:

$$1/t_h = 4\pi^2 V^2 / (h\gamma_0) \quad (19)$$

γ_0 is the coupling between the chromophore and its thermal bath and can be approximated by the Boltzmann factor kT .⁵¹ Table 6 shows the values of V deduced from the average values of hopping time determined according to the three models tested in the simulations. It can be seen that the more sophisticated the model, the closer the coupling values to those determined

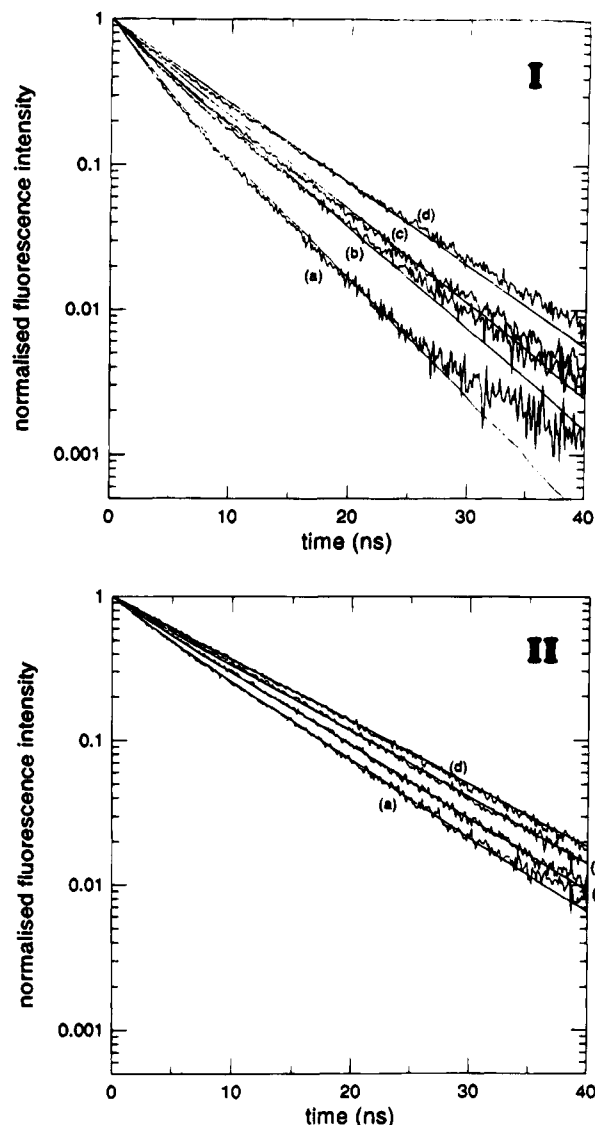


Figure 13. Fitting of experimental fluorescence decays recorded for the H5T (I) and H7T (II) mesophases with the simulated ones. Experimental conditions: TNF molar fraction (a) 5×10^{-3} , (b) 2×10^{-3} , (c) 10^{-3} , (d) 0; $\lambda_{\text{ex}} = 295$ nm; $\lambda_{\text{em}} = 400$ nm; $T = 80$ °C. Simulation parameters: fluorescence lifetime, 12.4 ns; intrinsic trap concentration, 10^{-3} ; column length, 1000 sites; hopping probability, varies with the distance as $p_z(R) = [1 - \exp(-aR^b)]^2 K/2R^6$ and $p_{xy}(R) = 7K[1 - \exp(-aR^b)]^2/4R^6$ ($a = 0.07$ and $b = 1.18$). The experimental curves are the noisy ones. The fits obtained for H9T are of the same quality as those of H7T.

TABLE 3: Hopping Time Values (ps) Determined by Fitting the Experimental Fluorescence Decay Curves with the Simulated Ones^a

TNF molar fraction	H5T	H7T	H9T
0	0.03	0.05	0.06
10^{-3}	0.03	0.07	0.20
2×10^{-3}	0.04	0.07	0.12
5×10^{-3}	0.05	0.12	0.16

^a Simulation parameters: hopping probability, varies with the distance as $1/R^6$; fluorescence lifetime, 12.4 ns; intrinsic trap concentration, 10^{-3} ; column length, 1000 sites.

either experimentally (10 cm^{-1}) or via quantum mechanical calculations (18 cm^{-1}). When the model used in simulations is the one corresponding to the extended dipole approximation and molecular orientation is taken into account, the values of the coupling determined for H5T, H7T, and H9T are 18, 13, and 11 cm^{-1} , respectively.

TABLE 4: Hopping Time Values (ps) Determined by Fitting the Experimental Fluorescence Decay Curves with the Simulated Ones^a

TNF molar fraction	H5T	H7T	H9T
0	0.11	0.25	0.30
10 ⁻³	0.14	0.38	0.70
2 × 10 ⁻³	0.18	0.40	0.47
5 × 10 ⁻³	0.22	0.60	0.63

^a Simulation parameters: hopping probability, $p_z(R) = K/2R^6$ and $p_{xy}(R) = 7K/4R^6$; fluorescence lifetime, 12.4 ns; intrinsic trap concentration, 10⁻³; column length, 1000 sites.

TABLE 5: Hopping Time Values (ps) Determined by Fitting the Experimental Fluorescence Decay Curves with the Simulated Ones^a

TNF molar fraction	H5T	H7T	H9T
0	0.38	0.80	0.90
10 ⁻³	0.52	1.15	2.40
2 × 10 ⁻³	0.64	1.20	1.50
5 × 10 ⁻³	0.78	1.90	2.10

^a Simulation parameters: hopping probability, $p_z(R) = K[1 - \exp(-aR^b)]^2/2R^6$ and $p_{xy}(R) = 7K[1 - \exp(-aR^b)]^2/4R^6$; fluorescence lifetime, 12.4 ns; intrinsic trap concentration, 10⁻³; column length, 1000 sites.

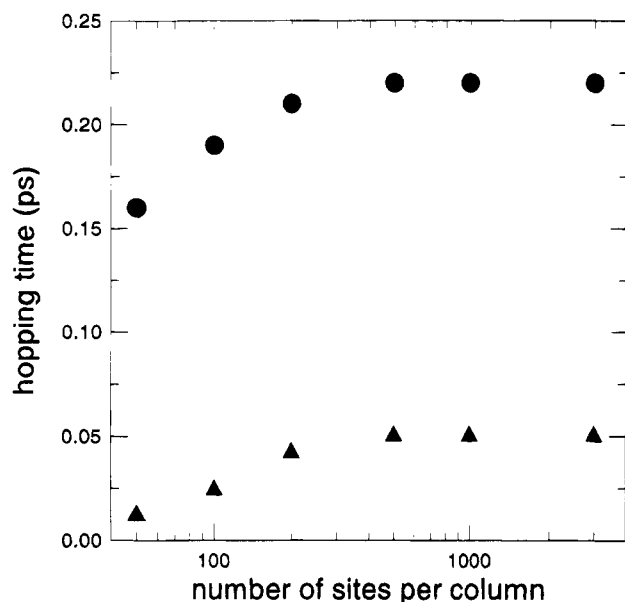


Figure 14. Influence of the column length on the hopping time. Simulation parameters: fluorescence lifetime, 12.4 ns; intrinsic trap concentration, 10⁻³; hopping probability, varies with the distance as (▲) $p_z(R) = p_{xy}(R) = 1/R^6$ or (●) $p_z(R) = K/2R^6$ and $p_{xy}(R) = 7K/4R^6$.

TABLE 6: Values of the Coupling (cm⁻¹) between Transition Moments of Nearest Neighbors Deduced from the Average Values of Hopping Time through Fermi's Golden Rule (eq 19)

model used in the simulations	H5T	H7T	H9T
dipole-dipole	70	50	39
dipole-dipole + molecular orientation	35	22	20
extended dipole + molecular orientation	18	13	11
quantum mechanical calculations		18	
experimental absorption spectra		10	

5. Summary and Conclusions

The main findings of our experimental and theoretical work concerning the excited states of 2,3,6,7,10,11-hexakis(alkyloxy)-triphenylenes (HrT) are the following.

The absorption maximum is due to the $S_0 \rightarrow S_4$ transition.

The $S_0 \rightarrow S_1$ transition is forbidden for chromophores having a threefold symmetry axis, but it becomes weakly allowed because of the alkoxy groups rotation and the vibronic coupling. The coupling between transition moments of two neighboring molecules in the same column, calculated according to the INDO formalism, is 700 and 18 cm⁻¹ for $S_0 \rightarrow S_4$ and $S_0 \rightarrow S_1$, respectively; the corresponding values evaluated from the experimental absorption spectra are 1000 ± 250 and 10 cm⁻¹. Thus, at the temperature domain of the mesophases, the $S_0 \rightarrow S_4$ transition corresponds to delocalized excited states while $S_0 \rightarrow S_1$ corresponds to localized ones. Moreover, calculation of intermolecular interactions shows that, in the liquid crystals, all the molecules, even those corresponding to structural defects, have the same excitation energy. Consequently no spectral diffusion of the fluorescence is expected, in agreement with the time-resolved emission spectra.

Energy transfer in the columnar mesophases is investigated by studying the fluorescence decays of mesophases doped with energy traps. The trap used is 2,4,7-trinitrofluoren-9-one (TNF), forming charge transfer complexes with HrT. Upon increasing the TNF concentration, the HrT fluorescence decays become more rapid; this variation depends on the lateral side chain length.

The analysis of the fluorescence decays is made by means of Monte Carlo simulations on the basis of a hopping mechanism, taking into account both intracolumnar and intercolumnar jumps and using four different models for the distance dependence of the hopping probability. When multipolar interactions are assumed within the column, no acceptable fit is obtained between experimental and simulated decay curves. Conversely, for dipolar interactions, the fits are relatively good and the hopping time is determined through the fitting procedure. It is shown that the more simplified the model used in the simulations the smaller the hopping time and, consequently, the bigger the coupling between nearest neighbors. As a matter of fact, if the molecules are considered as simple points, the hopping time values are found to be more than one order of magnitude smaller than those determined by taking into account molecular orientation and molecular dimensions. In the latter case (extended dipole approximation) the coupling values deduced from the hopping time are very close to those determined either experimentally or via quantum mechanical calculations.

In the analysis of both the excited states and the energy transfer, we have assumed that chromophores are static: all molecular vibrations and movements are neglected. The influence of these factors can be experimentally investigated by comparing the properties of columnar liquid crystals to those of the columnar glassy states where molecular movements are inhibited while the geometrical features of the organized system remain the same. Such a comparative study, carried out for other triphenylene derivatives than those studied in the present work, is now in progress.

Acknowledgment. This work has been performed in the frame of a European COST D4 project (Design and preparation of new molecular systems with unconventional electrical, optical and magnetic properties) entitled Columnar Liquid Crystals as Energy Guides for Molecular Electronics. The authors wish to thank Mr. P. Schuhmacher for support in the synthesis of hexakis(methyloxy)triphenylene and Dr. J. P. Lemaistre for helpful discussions.

References and Notes

- Chandrasekhar, S.; Sadashiva, B. K.; Suresh, K. A. *Pramana* **1977**, *9*, 471.
- Kreuder, W.; Ringsdorf, H. *Makromol. Chem. Rapid Commun.* **1983**, *4*, 807.

- (3) Levelut, A. M. *J. Chim. Phys.* **1983**, *80*, 149.
- (4) Chandrasekhar, S.; Ranganath, G. S. *Rep. Prog. Phys.* **1990**, *53*, 57.
- (5) Voigt-Martin, I. G.; Durst, H.; Brzezinski, V.; Krug, H.; Kreuder, W.; Ringsdorf, H. *Angew. Chem., Int. Ed. Engl.* **1989**, *28*, 323.
- (6) Markovitsi, D.; Rigaut, F.; Mouallem, M.; Malthête, J. *Chem. Phys. Lett.* **1987**, *137*, 236.
- (7) Blanzat, B.; Bartou, C.; Tercier, N.; André, J. J.; Simon, J. *J. Am. Chem. Soc.* **1987**, *109*, 6193.
- (8) Markovitsi, D.; Lécuyer, I.; Clergeot, B.; Jallabert, C.; Strzelecka, H.; Veber, M. *Liq. Cryst.* **1989**, *6*, 83.
- (9) Blasse, G.; Dirksen, G. J.; Meijerink, A.; Van der Pol, J. F.; Neelman, E.; Drenth, W. *Chem. Phys. Lett.* **1989**, *154*, 420.
- (10) Gregg, B. A.; Fox, M. A.; Bard, A. J. *J. Phys. Chem.* **1989**, *93*, 4227.
- (11) Markovitsi, D.; Lécuyer, I.; Simon, J. *J. Phys. Chem.* **1991**, *95*, 3620.
- (12) Markovitsi, D.; Lécuyer, I.; Lianos, P.; Malthête, J. *J. Chem. Soc., Faraday Trans.* **1991**, *87*, 1785.
- (13) Schouten, P. G.; Warman, J. M.; de Haas, M. P.; Fox, M. A.; Pan, H. L. *Nature* **1991**, *353*, 736.
- (14) Adam, D.; Closs, F.; Frey, T.; Funhoff, D.; Haarer, D.; Ringsdorf, H.; Shuhmacher, P.; Siemensmeyer, K. *Phys. Rev. Lett.* **1993**, *70*, 457.
- (15) Boden, N.; Bushby, R. J.; Clements, J. *J. Chem. Phys.* **1993**, *98*, 5920.
- (16) Bengs, H.; Closs, F.; Frey, T.; Funhoff, D.; Ringsdorf, H.; Siemensmeyer, K. *Liq. Cryst.* **1993**, *15*, 565.
- (17) Ecoffet, C.; Markovitsi, D.; Millié, P.; Lemaistre, J. P. *Chem. Phys.* **1993**, *177*, 629.
- (18) Ecoffet, C.; Markovitsi, D.; Jallabert, C.; Strzelecka, H.; Veber, M. *Thin Solid Films* **1994**, *242*, 83.
- (19) Ringsdorf, H.; Wüstefeld, R.; Zerta, E.; Ebert, M.; Wendorff, J. H. *Angew. Chem., Int. Ed. Engl.* **1989**, *28*, 914.
- (20) Kranig, W.; Boeffel, C.; Spiess, H.; Karthaus, O.; Ringsdorf, H.; Wüstefeld, R. *Liq. Cryst.* **1990**, *8*, 375.
- (21) Bengs, H.; Ebert, M.; Karthaus, O.; Kohne, B.; Praefcke, K.; Ringsdorf, H.; Wendorff, J. H.; Wüstefeld, R. *Adv. Mater.* **1990**, *2*, 141.
- (22) Bengs, H.; Karthaus, O.; Ringsdorf, H.; Baehr, C.; Ebert, M.; Wendorff, J. H. *Liq. Cryst.* **1991**, *10*, 161.
- (23) Markovitsi, D.; Bengs, H.; Ringsdorf, H. *J. Chem. Soc., Faraday Trans.* **1992**, *88*, 1275.
- (24) Metropolis, N.; Rosenbluth, A. W.; Teller, A. H.; Teller, E. *J. Chem. Phys.* **1953**, *6*, 1087.
- (25) Gould, H.; Tobochnik, J. *Computer Simulation Methods*; Addison-Wesley: Reading, MA, 1988.
- (26) Blumen, A.; Klafer, J.; Zumoffen, G. In *Optical Spectroscopy of Glasses*; Zschokke, I., Ed.; D. Reidel Publishing Co.: Dordrecht, The Netherlands, 1986; pp 199–265.
- (27) Billard, J.; Dubois, J. C.; Nguyen, H. T.; Zan, A. *Nouv. J. Chim.* **1983**, *2*, 807.
- (28) Bengs, H. Doctoral Dissertation, University of Mainz, 1993.
- (29) Velapoldi, R. A.; Mielenz, K. D. *NBS Spec. Publ.* **1980**, 260.
- (30) Berlman, I. B. *Handbook of Fluorescence Spectra of Aromatic Molecules*; Academic Press: New York, 1965.
- (31) Kruk, G.; Kocot, A.; Wrzalik, R.; Vij, J. K.; Karthaus, O.; Ringsdorf, H. *Liq. Cryst.* **1993**, *14*, 807.
- (32) Markovitsi, D.; Pfeffer, N.; Charra, F.; Nunzi, J. M.; Bengs, H.; Ringsdorf, H. *J. Chem. Soc., Faraday Trans.* **1993**, *89*, 37.
- (33) Momicchioli, F.; Balardi, I.; Bruni, M. C. *Chem. Phys. Lett.* **1983**, *82*, 229.
- (34) Momicchioli, F.; Balardi, I.; Berthier, G. *Chem. Phys.* **1988**, *123*, 103.
- (35) Arora, S.; Bates, R. B.; Goody, R. A.; Delfel, N. E. *J. Am. Chem. Soc.* **1967**, *89*, 4253.
- (36) Allen, F. H.; Kennard, O.; Watson, D. G.; Brammer, L.; Orpen, A. G.; Taylor, R. *J. Chem. Soc., Perkin Trans. 2* **1987**, S135.
- (37) Caillet, J. *Acta Crystallogr.* **1982**, *B38*, 1786.
- (38) Schaefer, T.; Laatikainen, R. *Can. J. Chem.* **1983**, *61*, 224.
- (39) Anderson, G. M., III; Kollman, P. A.; Domelsmith, L. N.; Houk, K. N. *J. Am. Chem. Soc.* **1979**, *101*, 2344.
- (40) Goldfarb, D.; Luz, Z.; Zimmermann, H. *J. Phys. (Paris)* **1981**, *42*, 1303.
- (41) Marguet, S.; Mialocq, J. C.; Millié, P.; Berthier, G.; Momicchioli, F. *Chem. Phys.* **1992**, *160*, 265.
- (42) Chojnacki, H.; Laskowski, Z.; Lewanowicz, A.; Ruziewicz, Z.; Wandas, R. *Chem. Phys. Lett.* **1986**, *124*, 478.
- (43) Levelut, A. M. *J. Phys. Lett.* **1979**, *40*, L-8.
- (44) Frenkel, J. *Phys. Rev.* **1931**, *37*, 1276.
- (45) Davydov, A. S. *Theory of Molecular Excitons*; Plenum Press: New York, 1971.
- (46) Rashba, E. I.; Sturge, M. D. *Excitons*; North-Holland Publishing Company: Amsterdam, The Netherlands 1982.
- (47) Claverie, P. In *Intermolecular Interactions: from Diatomics to Biopolymers*; Pullman, B., Ed.; Milley: New York, 1978.
- (48) Czikkleky, V.; Försterling, H. D.; Kuhn, H. *Chem. Phys. Lett.* **1970**, *6*, 207.
- (49) Scholes, G. D.; Ghiggino, K. P. *J. Phys. Chem.* **1994**, *98*, 4580.
- (50) Maitland, G. C.; Rigby, M.; Smith, E. B.; Wakeham, W. A. *Intermolecular Forces*; Clarendon Press: Oxford, U.K., 1981; p 51.
- (51) Brown, R.; Lemaistre, J. P.; Megel, J.; Pée, P.; Dupuy, F.; Kottis, P. *J. Chem. Phys.* **1982**, *76*, 5719.